RSC Advances

ROYAL SOCIETY OF CHEMISTRY

PAPER

View Article Online
View Journal | View Issue

Check for updates

Cite this: *RSC Adv.*, 2025, **15**, 6457

Doxorubicin-loaded pH-responsive porphyrin-derived carbon dots as a promising biocompatible drug delivery system for effective chemotherapy of breast cancer†

Abeer Ansary,[a,b] Ahmed Osman[a] and Mohamed E. El-Khouly *[c]

Received 28th December 2024
Accepted 18th February 2025

DOI: 10.1039/d4ra09058f

rsc.li/rsc-advances

Doxorubicin (DOX), a widely used chemotherapy drug for breast cancer, suffers from limitations such as non-specific toxicity and drug resistance. To address these challenges, we developed a novel drug delivery system (DDS) using porphyrin-derived carbon dots (CDs) as carriers for DOX. Porphyrin-based CDs were synthesized solvothermally from tetrakis(4-carboxyphenyl) porphyrin (TCPP) and urea. DOX was non-covalently loaded onto the CDs to form the DOX@CDs nanocomposite. The resulting CDs exhibited desirable properties like excellent water solubility, stability, and biocompatibility. Moreover, the DOX@CDs complex showed a high drug loading efficiency of 93% and a pH-responsive release profile, with enhanced release at acidic tumor microenvironments. The DOX@CDs nanocomposite demonstrated significantly improved cytotoxicity against human breast cancer MCF-7 and MDA-MB-231 cell lines (at IC_{50} values 24.08 ± 1.446 and 10.587 ± 0.815 $\mu g\ mL^{-1}$) compared to free DOX (at IC_{50} values = 262.96 ± 1.807 and 261.6 ± 0.907 $\mu g\ mL^{-1}$). Analysis by fluorescence microscopy and flow cytometry demonstrated that the enhanced cytotoxicity of the DOX@CDs complex compared to free DOX correlated with its greater cellular uptake and localization in cancerous cells. Notably, the nanocomposite exhibited reduced hemolytic activity, indicating enhanced biocompatibility. Our findings suggest that porphyrin-derived CDs hold promise as a safe and effective nanocarrier for targeted DOX delivery, offering a potential strategy to improve the therapeutic efficacy of breast cancer chemotherapy.

1 Introduction

Breast cancer (BC) remains a significant global health concern, particularly among women. Despite advancements in treatment, the aggressive nature of the disease and the development of drug resistance continue to hinder therapeutic outcomes.[1] In 2022, BC was the second most diagnosed cancer worldwide, affecting millions of women moreover, it was the fourth leading cause of cancer-related deaths. A approximately 30% of early-stage BC cases progress to metastatic disease highlighting the urgent need for innovative therapeutic strategies.[2] While systemic therapies are employed for both early-stage and metastatic BC, the primary goal for metastatic breast cancer (MBC) is to control disease progression, extend survival, and improve quality of life.[1]

Doxorubicin (DOX) remains a cornerstone chemotherapy for breast cancer (BC), but its clinical utility is hampered by drug resistance, systemic toxicity, and lack of tumor selectivity.[3,4] To address these limitations, the utilization of novel nanocarriers offers a promising approach to enhance DOX's therapeutic efficacy and reduce adverse effects.[5,6] Nanocarriers, including inorganic nanoparticles (*e.g.*, gold, iron oxide), organic nanoparticles (*e.g.*, polymers, liposomes, micelles), and hybrid systems, can improve DOX's pharmacokinetics, biodistribution, and tumor targeting.[7,8] While liposomal DOX (LD) and pegylated liposomal DOX (PLD) have achieved clinical success, ongoing research explores a diverse range of nanocarrier platforms to further optimize DOX delivery and improve patient outcomes.[9]

Among the carbon-based organic nanoparticles, zero-dimensional carbon dots (CDs) have emerged as promising nanocarriers for drug delivery systems (DDS) due to their exceptional properties: high biocompatibility, low toxicity, good water solubility, and unique optical properties.[10] These characteristics have led to their widespread application in bioimaging, biosensing, drug delivery, and photocatalysis.[11] The synthetic

---

[a] *Biotechnology Program, Institute of Basic and Applied Science, Egypt-Japan University of Science and Technology, New Borg El-Arab City, Alexandria, Egypt*

[b] *Department of Biochemistry, Faculty of Pharmacy, Kafrelsheikh University, Kafrelsheikh, Egypt*

[c] *Nanoscience Program, Institute of Basic and Applied Science, Egypt-Japan University of Science and Technology, New Borg El-Arab City, Alexandria, Egypt. E-mail: mohamed.elkhouly@ejust.edu.eg*

† Electronic supplementary information (ESI) available. See DOI: **https://doi.org/10.1039/d4ra09058f**

approach and precursor choice significantly influence the surface functionality of CDs, enabling post-synthesis modifications through covalent or noncovalent interactions with therapeutic and targeting moieties.[12] Porphyrin derivatives are ideal precursors for carbon dot (CD) synthesis due to their unique tetrapyrrole structure, strong π–π conjugated system, and inherent optical and photochemical properties. The presence of functional groups (hydroxyl, carboxyl, amino) on the porphyrin structure allows for the formation of CDs with characteristic surface functionalities, enhancing stability, biocompatibility, and facilitating conjugation with other molecules without further modification. This eliminates the need for additional passivation steps often required with conventional carbon sources.[13–15] For example, red-emissive CDs derived from TCPP and thiourea have been successfully employed as probes for Hg^{2+} and glutathione detection, while porphyrin-derived CDs have been developed for photodynamic therapy applications.[16,17]

Taking these unique features into consideration, we report the synthesis and characterization of porphyrin-derived carbon dots (CDs) using TCPP as a carbon source and urea as a doping agent. These CDs were evaluated as a biocompatible nanocarrier for doxorubicin (DOX). The physicochemical properties, drug loading capacity, release kinetics, and biocompatibility of DOX@CDs were characterized.

2 Materials and methods

2.1. Materials

Urea, TCPP, DOX hydrochloride (DOX·HCL), *N*,*N*-dimethylformamide (DMF), perinaphthenone, acetonitrile, dimethyl sulfoxide (DMSO), and 3-(4,5-dimethylthiazol-2-yl)-2,5-diphenyltetrazolium bromide (MTT) were purchased from Sigma-Aldrich, Inc. (St. Louis, Missouri, USA). The dialysis tubing with molecular-weight cutoffs (MWCO) 1000 and 3500 dalton was obtained from FREY Scientific, Inc. (Northwest Blvd, Nashua, NH 03063, USA). Cell culture plastics and culture wares were purchased from Greiner Bio-One GmbH (Bad Haller Str. 32, Kremsmünster, Austria). Dulbecco's Modified Eagle Medium (DMEM), fetal bovine serum (FBS), 0.25% trypsin–EDTA, phosphate buffer saline (PBS), and penicillin/streptomycin antibiotics were provided by Gibco (Grand Island, NY, USA). Breast cancer (MCF-7 and MDA-MB-231) and normal human retinal pigment epithelial-1 (RPE-1) cell lines were acquired from Nawah Scientific (Mokatam, Cairo, Egypt). The remaining chemicals and reagents utilized in this investigation were obtained from the El-Gomhouria Company for selling Chemicals and Medical Appliances (Cairo, Egypt).

2.2. Fabrication of porphyrin-based CDs and DOX@CDs complex

The CDs were synthesized solvothermally starting with TCPP and urea following the procedure previously described by Zeng *et al.*, where 1 g of urea and 10 mg of TCPP were stirred together in 10 mL DMF until dissolution and then transferred into a Teflon-lined autoclave to be heated for 4 h at 180 °C. Subsequently, the obtained solution was left to cool at room temperature, centrifuged, and filtered. The clear supernatant was then dialyzed against deionized water using the dialysis bag (MWCO = 1000 Da) for 24 h with changing the outer medium every 4 h, and the resulting purified CDs solution was then frozen for lyophilization. After that, the final dried CD powder was stored and kept at 4 °C for subsequent use.[16]

Concerning DOX@CDs nanocomposite preparation, DOX was loaded into CDs through the noncovalent approach as previously reported,[12] where 8 mg of CDs dissolved in 1 mL PBS (pH = 7.4) and 0.4 mg of DOX dissolved in 1 mL PBS (pH = 7.4) were mixed and completed up to 4 mL with PBS. This electrostatic interaction was left on the stirrer for 48 h at 400 rpm and 25 °C. The solution was then dialyzed against deionized water using a dialysis bag (MWCO = 3500 Da) to eliminate the excess unreacted CDs or DOX. Importantly, both the loading and dialysis steps were performed under dark conditions to avoid the degradation of DOX by the light effect. Finally, the as-prepared solution was dried by lyophilization, and the resulting powder was stored at 4 °C right the photochemical characterization and biological assays.

2.3. Characterization of CDs, DOX, and DOX@CDs complex

The optical properties of all samples were investigated using a UV-2600 spectrophotometer (Shimadzu, Japan) for UV-vis absorbance and an RF6000 spectrofluorometer (Shimadzu, Japan) for emission spectroscopy in deionized water. Infrared (IR) spectra were recorded on an Alpha IR 100 FT-IR spectrometer (Bruker, Germany) in the range of 4000–400 cm^{-1}. The morphology, particle size distribution, and elemental composition of the porphyrin-based carbon dots (CDs) were characterized by transmission electron microscopy (TEM) using a JEM-2100Plus instrument (JEOL, Japan). The zeta potential of all samples was measured in deionized water using a Zetasizer nano Ver. 7.02 (Malvern, United Kingdom).

2.4. Calculation of CDs' fluorescence quantum yield and lifetime

The fluorescence quantum yield (Φ_f) of porphyrin-derived CDs was determined as previously described[18,19] using the tris(bipyridine) ruthenium(II) chloride ($[Ru(bpy)_3]Cl_2$) as a reference (Φ_s = 4% in deionized water),[20] where the UV absorbance for both CDs and reference was recorded in deionized water at 419 nm, and their emission spectra were also recorded at the same excitation wavelength of 419 nm. Followingly, the quantum yield value of the CDs was calculated by applying the eqn (1).

$$\Phi_s = \Phi_r \times \frac{F_s}{F_r} \times \frac{A_r}{A_s} \tag{1}$$

Φ_s and Φ_r represents the quantum yields of the sample and reference, respectively. F_s and F_r are the integration of the sample and reference emission spectra, respectively. A_r and A_s representing the optical density (at 419 nm) of the reference and sample, respectively.

Fluorescence lifetime measurements were performed by exciting TCPP and CDs at 439 nm with a NanoLED pulsed diode light source (HORIBA Scientific). The resulting fluorescence decay curves were then analyzed using the 64 decay analysis software (HORIBA Scientific) to determine the fluorescent lifetimes.[21]

2.5. Assessment of CDs' fluorescence- and photo-stability

The fluorescence stability of the synthesized CDs under different cell culture conditions (PBS, plain cell culture medium, and complete cell culture medium with 10% serum) utilizing deionized water as control was evaluated by recording their emission spectra after incubation at different time intervals using an RF6000 spectrofluorometer (Shimadzu, Japan). To assess the photostability of CDs, their UV-vis absorption spectra were recorded every 2 minutes for 24 minutes. Prior to each measurement, the CD solution in phosphate-buffered saline (PBS) was irradiated with a xenon arc lamp (Shimadzu RF6000 spectrofluorometer) for 1 minute. Spectral analysis was performed using a Shimadzu UV-2600 spectrophotometer.

2.6. Assessment of CDs' solubility and stability in water

To evaluate the water solubility and stability of the fabricated porphyrin-based carbon dots (CDs), dynamic light scattering (DLS) using a Zetasizer nano Ver. 7.02 (Malvern, United Kingdom) and UV-vis spectroscopy were employed, respectively. Stock DMSO solutions of the CDs and the starting porphyrin were diluted to 0.1% in phosphate-buffered saline (PBS) for DLS analysis. To assess the CDs' stability under physiological conditions, CD powder was dissolved in PBS, and its UV-vis absorption spectrum was recorded daily for four days.

2.7. Determination of CDs' partition coefficient

The CDs' lipophilicity was assessed by applying the "shake-flask" method to determine the partition coefficient ($\log P$) between an aqueous phase (PBS) and an organic phase (octanol) as previously described.[22] In this approach, both phases were pre-saturated with each other and left to separate. The sample was then dissolved in its favorable solvent along with an equal volume of other solvent and left for shaking overnight. On the next day, the mixture was left until complete separation, followed by measuring the sample absorbance in both phases at three replicates utilizing a UV-2600 spectrophotometer (Shimadzu, Japan). The average concentration of the sample in each solvent was calculated and applied to calculate the $\log P$ value according to eqn (2).

$$\log P = \log \frac{C_{\text{org}}}{C_{\text{aq}}} \tag{2}$$

C_{org} and C_{aq} are the concentrations of the sample in organic and aqueous phases, respectively.

2.8. Assessment of DOX loading quality into porphyrin-based CDs

DOX loading efficiency (DLE) and DOX loading capacity (DLC) were measured spectrophotometrically as reported by Kong *et al.*[6] Firstly, a standard calibration curve was prepared using a set of known serial concentrations of DOX. Then, the unknown amount of DOX loaded onto the CDs was calculated by measuring the DOX absorbance at 481 nm. By implementing the straight-line equation extracted from the calibration curve, the DLE and DLC were calculated according to eqn (3) and (4), respectively.

$$\text{DLE}(\%) = \frac{\text{Amount of DOX loaded in CDs}}{\text{Initial amount of the DOX}} \times 100 \tag{3}$$

$$\text{DLC}\left(\text{mg g}^{-1}\right) = \frac{\text{Amount of DOX loaded in CDs}}{\text{Initial amount of CDs}} \tag{4}$$

2.9. *In vitro* pH-dependency of DOX release and kinetics

The pH-dependent DOX release experiment was performed as prescribed previously,[6] where a dialysis bag (MWCO = 1000) containing 5 mL of DOX@CDs solution was immersed against 100 mL of PBS at three different pH conditions (pH = 7.4, 5.0, and 6.8). These release solutions were then left inside the shaker incubator at 37 °C and 200 rpm under dark conditions to simulate the *in vivo* system of drug release. At each specified time interval, 2.0 mL (at three replicates) from the released solution was removed and substituted by an equal volume of new PBS. The absorbance of those aspired solutions at different time intervals was measured to quantify the amount of DOX released by applying the straight-line equation extracted from the previously graphed calibration curve. Finally, the DOX release percentage was calculated according to eqn (5).

$$\text{DOX release}(\%) = \frac{\text{DOX amount in release medium}}{\text{Total amount of DOX loaded into CDs}} \times 100\% \tag{5}$$

For a deeper insight into the kinetic mechanism by which DOX is released from porphyrin-based CDs, different drug release models[18] were applied in this study as shown below:

Zero-order model eqn (6):

$$Q_t = Q_0 + K_0 t \tag{6}$$

where Q_t is the drug fraction released per unit time (t), Q_0 is the initial drug amount at zero time, and K_0 is the constant of the zero-order release model.

First-order model eqn (7):

$$\text{Log}\, Q_t = \log Q_0 - K_t/2.303 \tag{7}$$

where Q_t is the drug fraction released per unit time, Q_0 is the initial drug amount at zero time, and K_t is the first-order release model constant.

Korsmeyer–Peppas model eqn (8):

$$\text{Log}(M_t/M_\infty) = \log k + n \log t \tag{8}$$

where M_t and M_∞ are the released amount of the drug at a certain time (t) and infinite time (∞), respectively, k is the

Korsmeyer–Peppas kinetic constant, and n is the exponent of drug release (indicator for the drug diffusion mechanism).

2.10. Cytotoxicity assay (MTT test)

The MTT test was performed according to the previously reported protocols to investigate the biocompatibility and the cytotoxicity of the studied compounds.[12,18] In this assay, all compounds were examined against MCF-7, MDA-MB-231, and RPE-1 cell lines. The assay was performed in a 96-well plate, where 100 μL suspension of each cell line was cultivated at 6×10^3 cells per well and left overnight inside the incubator at 37 ° C, 5% CO_2, and 95% humidity to allow their adherence to the well surface. On the next day, stock solutions of CDs, free DOX, and DOX@CDs (the same concentration as free DOX was conserved), and subsequently RPE-1 cells were exposed to 100 μL culture medium of either of the studied compounds at five ascending concentrations of 6.25, 12.5, 25, 50, and 100 μg mL^{-1}, while for the MCF-7 and MDA-MB-231 cells, 100 μL culture medium of either of the studied compounds at concentrations of 1.9, 3.8, 7.8, 15.6, 31.2, 62.5, 125, 250, and 500 μg mL^{-1} were applied (each concentration was applied at 3 replicates). After an incubation period of 48 hours, 50 μL of MTT solution (2.5 mg mL^{-1}) was added to each well, followed by incubation for a further two hours. Then, the medium in each well was exchanged by DMSO (200 μL) to dissolve the formed formazan crystals. The optical density (OD) was recorded at 570 nm using a microplate reader (Tecan) and cell viability (%) of treated cells was then calculated using the OD of untreated cells as a reference point as shown in eqn (9), while the half-maximal inhibitory concentration (IC_{50}) was determined using GraphPad Prism software (version 8.0.1).

$$\text{Cell viability }(\%) = \text{OD of treated cells}/\text{OD of untreated cells} \times 100 \quad (9)$$

2.11. Intracellular uptake

The cellular uptake of CDs, free DOX, and DOX@CDs composite into breast cancer cell lines MCF-7 and MDA-MB-231 were evaluated at both quantitative and qualitative levels using flow cytometry and fluorescence microscopy, respectively as previously reported.[6,23,24] Firstly, the MCF-7 and MDA-MB-231 cells were cultivated overnight in 6-well plates overnight at 5 × 105 and 2 × 105 cells per well, respectively. The day next, CDs, free DOX, and DOX@CDs composite were applied to both cells (the MCF-7 and MDA-MB-231) at the same concentrations of 250 μg mL^{-1} (CDs) and 260 μg mL^{-1} of DOX (for free DOX and DOX@CDs) followed by incubation at different times (2 and 4 hours). Fluorescence imaging was monitored after 4 hours of incubation depending on the self-fluorescence of the compounds studied, where the medium was discarded followed by washing the cells with PBS (3 times) to remove any residual particles or medium. Followingly, the images were captured under both green and red-light using ZOE Fluorescent Cell Imager (BIO-RAD, Singapore). The flow cytometry analysis was performed after incubation times 2 and 4 hours, where cells were washed with PBS followed by trypsinization using trypsin–EDTA and centrifugation (1000 rpm for 5 minutes). Then, the collected cell pellets were washed 3 times with PBS to remove any medium followed by resuspension in PBS (500 μL). Lastly, the cellular uptake was quantified by a BD FACSLyric flow cytometer (BD Biosciences, USA).

2.12. Hemolysis test

The biocompatibility of the fabricated CDs and DOX@CDs in comparison with the free DOX was further investigated through the hemolysis assay which was performed by following the previously reported procedures.[25–28] Herein, a freshly collected 5 mL blood sample from a rabbit was combined with 5 mL PBS (pH = 7.4), centrifuged at 3000 rpm for 15 min, and followed by discarding the clear supernatant, leaving the red blood cells (RBCs) precipitate. This step was repeated three times for washing and purifying the RBCs. The purified RBCs were then diluted with PBS to a final concentration of 2% (v/v). On the other hand, various concentrations at 50, 100, 200, and 400 μg mL^{-1} of CDs, while at 10, 20, 30, and 40 μg mL^{-1} of DOX for both free DOX and DOX@CDs were prepared. Then, 500 μL of the tested compound was thoroughly mixed with 500 μL of PBS, 500 μL of deionized water, and 500 μL of RBCs' suspension, followed by incubation at 37 °C for 4 hours. The mixtures were then centrifuged at 3000 rpm for 15 min, followed by arranging each group in an ascending order of concentrations to photograph the hemolytic effect. The clear supernatants were then collected to measure the absorbance value (Abs.) of the released hemoglobin at 540 nm using the UV-2600 spectrophotometer (Shimadzu, Japan). The test was performed under the same conditions for the negative and positive controls, but the tested sample was replaced by PBS and deionized water, respectively. This test was performed at three replicates, under the same conditions, for each concentration of the tested samples as well as the negative and positive control groups. The hemolysis ratio was calculated according to eqn (10).

$$\text{Hemolysis ratio}(\%) = \frac{\text{Abs. of sample} - \text{abs. of negative control}}{\text{Abs. of positive control} - \text{abs. of negative control}} \times 100 \quad (10)$$

2.13. Statistical analysis

Statistical analysis of the data generated was performed using OriginPro 2024 and GraphPad Prism 8.0.1. Results are presented as mean ± SD. The analysis of variance (ANOVA) was used to determine statistical significance ($p < 0.05$) among groups.

3 Results and discussion

3.1. Fabrication of porphyrin-based CDs and DOX loading into the synthesized CDs

Porphyrin-derived carbon dots (CDs) were synthesized *via* a facile, one-step solvothermal method, employing urea as

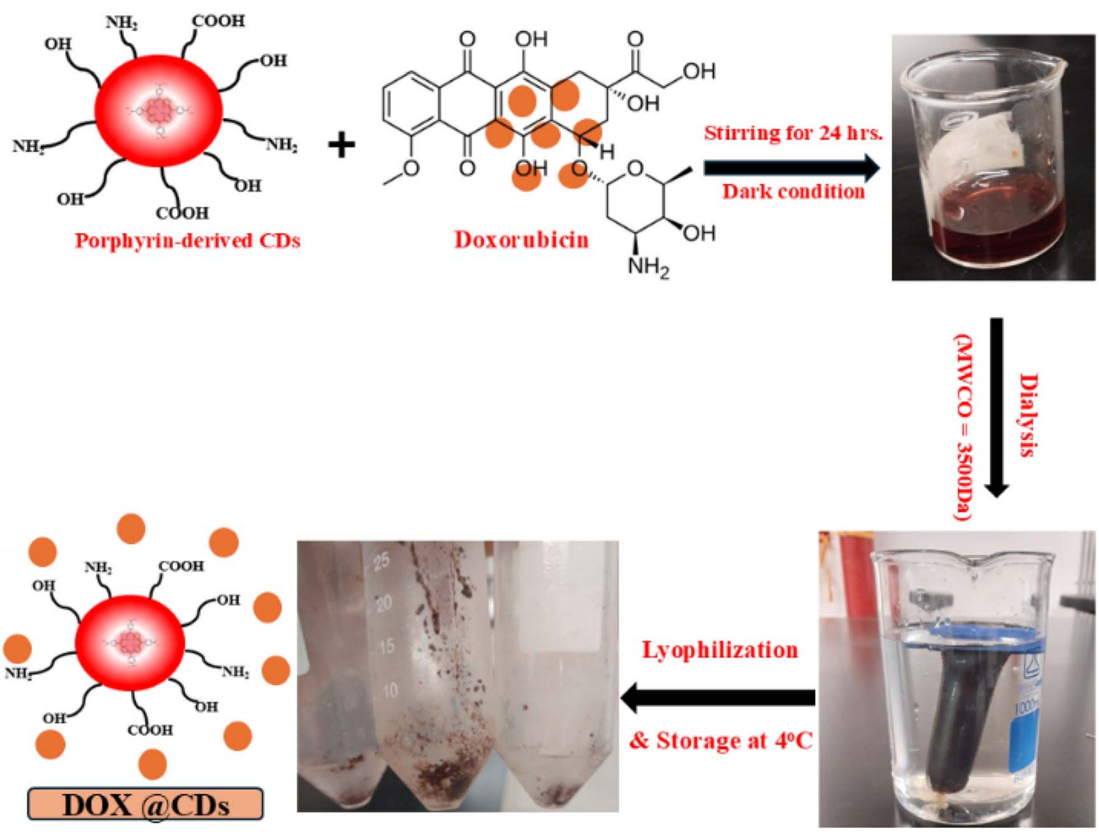

Fig. 1 Simplified illustration of the non-covalent loading of DOX into the fabricated porphyrin-derived CDs.

a doping agent (Fig. S1†).[16] We utilized urea in our study as a doping agent in fabricating the examined CDs because of its abundant availability, cost-effectiveness, little toxicity, and low corrosiveness.[29] The as-prepared CDs were used as a non-covalent carrier for doxorubicin (DOX), leveraging electrostatic interactions, as illustrated in Fig. 1. This non-covalent strategy was chosen for its simplicity, efficient drug release, and enhanced therapeutic efficacy against cancer cells.[12]

3.2. Morphological, chemical, and photophysical characterization of porphyrin-based CDs and DOX@CDs nanocomposite

The TEM analysis demonstrated that the fabricated porphyrin-derived CDs possessed a desirable spherical morphology (Fig. 2a) and a uniform size distribution ranging from 2.8 to 9.4 nm, with an average diameter of 6.41 ± 1.59 nm (Fig. 2b). EDX mapping analysis revealed that the primary constituents of the as-prepared CDs were carbon (92.06%), oxygen (4.88%), and nitrogen (3.06%) (Fig. 2c). These findings suggest that carbon constitutes the majority of the CDs' framework, while oxygen and nitrogen contribute to a lesser extent.

To further characterize the surface coating of the CDs and DOX@CDs nanocomposite, we performed zeta potential analysis at a concentration of 0.1 mg mL^{-1} and a pH value of 7. This technique provides insights into the type and quantity of surface charges, as well as the stability of DOX loading on the CDs.[18,30] As shown in Fig. S2,† the zeta potential of porphyrin-derived CDs was −40.5 mV, consistent with previous studies attributing the high negative charge to the ionized carboxylic groups of the porphyrin molecule.[31] On the other hand, the DOX@CDs complex had a zeta potential value of −37.2 mV. The increase in CDs' zeta potential after DOX loading is likely due to electrostatic interactions between the CDs' carboxylic groups and the amino groups of DOX·HCl, as well as hydrogen bonding during the non-covalent coupling.[18] The zeta potential of the DOX@CDs complex below −30 mV indicates successful DOX loading and reasonable stability of the composite, as reported previously.[23,32]

In addition, the FT-IR analysis was performed to investigate the surface doping of porphyrin-based CDs with urea and to verify the loading of as-prepared CDs by DOX. As shown in Fig. 3a, porphyrin and CDs' spectra exhibited absorption bands ranging from 3100 to 3400 cm^{-1}, which denoted O–H/N–H stretching. In addition, the TCPP spectrum displayed bands at 1684, 1222, and 790 cm^{-1} which could be assigned to C═C stretching, C–N stretching, and C–H bending vibration, respectively, while the CDs' spectrum displayed a characteristic absorption peak at 1654 cm^{-1}, which could be referred to the amide bond (–CO–NH–) stretching, in addition to the bands at 1595, 1148, 1103, and 775 cm^{-1} are typically characteristic for the C═C stretching, C–N stretching, C–O stretching, and C–H bending vibrations, respectively. These results depicted the successful surface functionalization of the fabricated CDs with

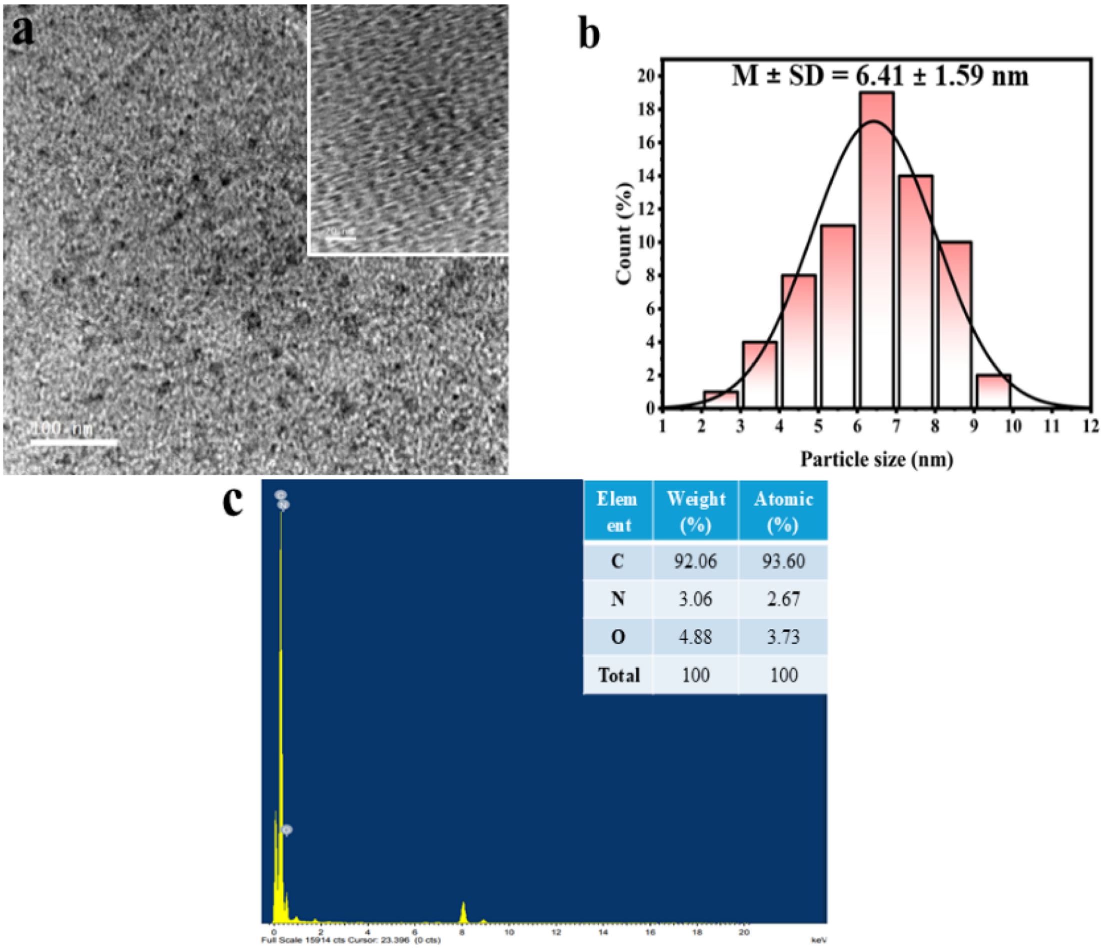

Fig. 2 (a) Structural morphology of the fabricated porphyrin-derived CDs (TEM image 100 nm scale) and the enclosed photograph represent the high-resolution TEM imaging of the CDs at 20 nm scale. (b) Histogram of the CDs' particle size distribution. (c) EDX mapping analysis of the CDs' elemental composition. The inset table represents the atomic and weight percentages of each element.

oxygen-rich and nitrogen-rich groups such as –OH, –COOH, and amino groups, in addition, they could propose the hydrophilic properties of the synthesized CDs as well as their validity for the non-covalent complexation with DOX as previously reported.[23,33] For DOX and DOX@CDs composite spectra (Fig. 3b), both free DOX and DOX@CDs composite displayed absorption bands at 3433 and 3436 cm^{-1}, respectively which correspond to the O–H/N–H stretching vibration, in addition, the C=O stretching band appeared at 1637 and 1641 cm^{-1}, respectively. The free DOX spectrum also exhibited bands at 1214, 1074, 784, and 705 cm^{-1} that were assigned to –C–O–C– stretching, C–H bending, and C=C ring bending, respectively, while the DOX@CDs complex exhibited bands at 1384, 1085, and 529 cm^{-1} that could be referred to C–N stretching, C–O stretching, and C–H bending, respectively. Notably, findings are also consistent with the previously reported studies concerning the electrostatic interaction between DOX and CDs for the successful design of DOX@CDs nanocomposite.[6,12,23]

The UV-vis absorption and emission spectra were recorded to further understand the optical behaviors of the newly fabricated CDs and DOX@CDs complex. Concerning the UV-vis absorption spectra as shown in Fig. 3c, the TCPP and CDs exhibited an identical characteristic Soret band at 419 nm, which implies that, even after the solvothermal reaction under high temperature and pressure, the intrinsic core structure of the starting porphyrin molecule was preserved.[16] However, the CDs displayed an extra peak at around 260 nm which is more likely due to the π–π* transition of the C=C bond that is characteristic of CDs.[18,34] More importantly, the DOX@CDs spectrum also displayed the same characteristic peak of TCPP and CDs at 419 nm, but with lower intensity compared to that of the CDs, in addition, the DOX@CDs spectrum showed the characteristic peak of DOX at 481 nm with lower intensity as well when compared to that of DOX alone which displayed a strong absorption peak at 481 nm. These findings revealed that there was a certain degree of mutual quenching of both the CDs and DOX absorption in the DOX@CDs complex, which subsequently verified the successful loading of DOX onto the porphyrin-based CDs.[6,35]

The photoluminescence (PL) behavior of the fabricated CDs is demonstrated in Fig. S3,† where porphyrin-based CDs exhibited an excitation-independent emission through a range

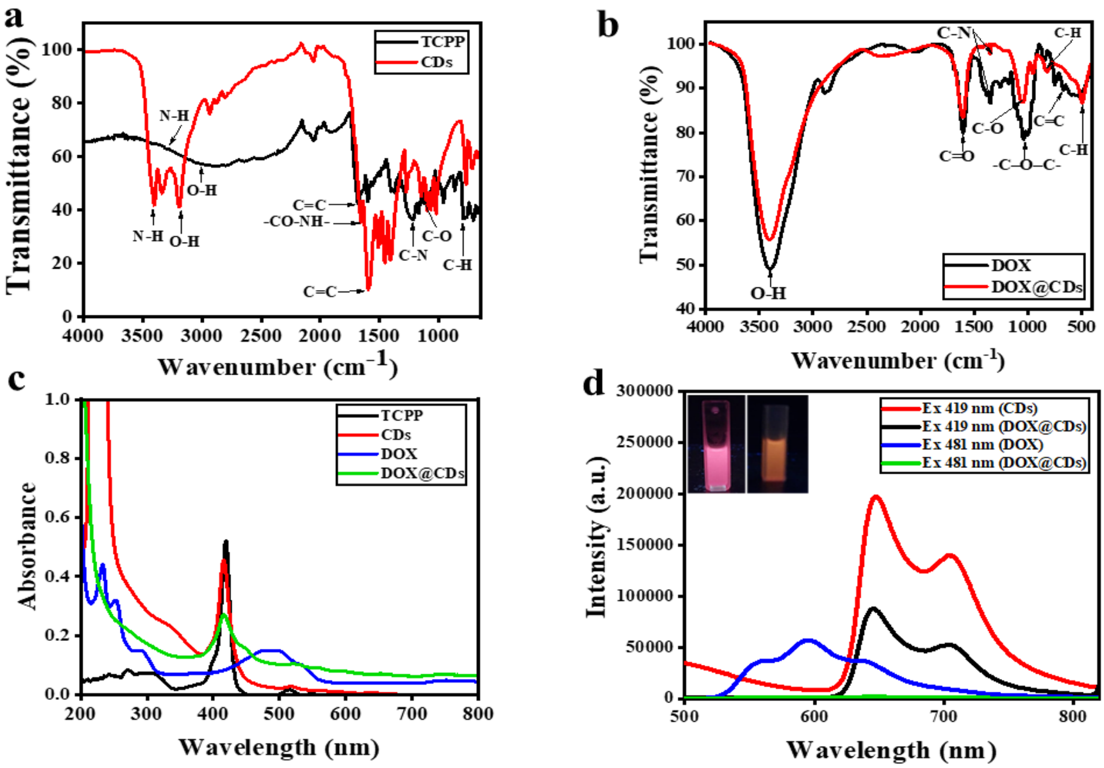

Fig. 3 Comparative FT-IR spectra of starting porphyrin and the resultant CDs (a) as well as DOX and DOX@CDs complex (b). UV-vis absorption spectra of porphyrin, CDS, DOX, and DOX@CDs (c). Emission spectra of free CDs, free DOX, and DOX@CDs complex; $\lambda_{ex} = 419$ and 481 nm. Emission spectra of CDs; λ_{ex}= 419 nm, free DOX; λ_{ex}= 481nm, and DOX@CDs complex; λ_{ex}= 419 and 481 nm (d). Insets: DOX@CDs' solution (left) and free DOX solution (right) under UV-lamp at 365 nm.

from 360–460 nm with a maximum emission intensity at 650 nm in response to an excitation wavelength at 419 nm which is typically identical to the emission attitude of the starting porphyrin molecule as previously reported.[36] Additionally, the as-prepared CDs exhibit a transparent pale pink solution under daylight (left), while a strong red fluorescence under a UV lamp at 365 nm (right) as demonstrated in the inset image of Fig. S3.† The fluorescence quantum yield of the synthesized CDs in deionized water was found to be 2.3% using tris(bipyridine) ruthenium(II) chloride ($[Ru(bpy)_3]Cl_2$) as a reference ($\Phi_f = 4\%$ in deionized water). Moreover, the fluorescence lifetime of both the starting porphyrin and the as-prepared CDs was calculated to show the difference in their decay behavior. As shown in Fig. S4,† the singlet-excited TCPP (in DMF at 650 nm) exhibited a mono-exponential decay function with a lifetime value of 8.33 ns. On the contrary, the singlet-excited CDs (in deionized water at 650 nm) displayed a bi-exponential fast and slow decay. The fast-decay behavior had a lifetime value of 1.89 ns (with a ratio of 20%), which could be attributed to the surface functional groups of the CDs, while the slow-decay behavior with a lifetime decay of 7.99 ns (with a ratio of 80%) which approximately equals the lifetime decay of TCPP and could be ascribed to the core state of the CDs.[33,37] These results are consistent with the above-mentioned findings indicating that the intrinsic core structure of TCPP was maintained.[16]

On the other hand, by comparing the PL behavior of the free DOX, free CDs, and DOX@CDs complex as shown in Fig. 3d, it was revealed that the emission characteristic peak of free DOX at 595 nm in response to an excitation at 481 nm disappeared in the DOX@CDs' spectrum when excited at the same 481 nm wavelength. In addition, the intensity of fabricated CDs' characteristic emission peak at 650 nm has been quenched in the presence of DOX as compared to that of CDs alone. This mutual quenching effect was also noticed by examination under the UV lamp at 365 nm as shown in the inset image of Fig. 3d. Taken together, these data verified the successful noncovalent loading of DOX into those newly synthesized CDs which are compatible with the previously reported studies.[6,12,23]

The fluorescence stability of CDs is considered a prerequisite for their biomedical applications. Herein, we further evaluated the PL behavior of the newly synthesized porphyrin-derived CDs under different cell culture conditions. Overall, along the different measurement times starting from time zero until 8 hours under incubation with various media using deionized water as a control, there was a negligible change in the maximum emission intensity at 650 nm upon excitation at 419 nm, indicating the CDs' stability under physiological conditions. However, compared to the fluorescence intensity values in deionized water (control) during the total measurement period, there was an enhancement in the fluorescence intensities under incubation with other utilized cell culture media (Fig. 4). These findings could be attributed to many factors including the surface functional groups like amino, carboxyl, and hydroxy groups which prevent aggregation and

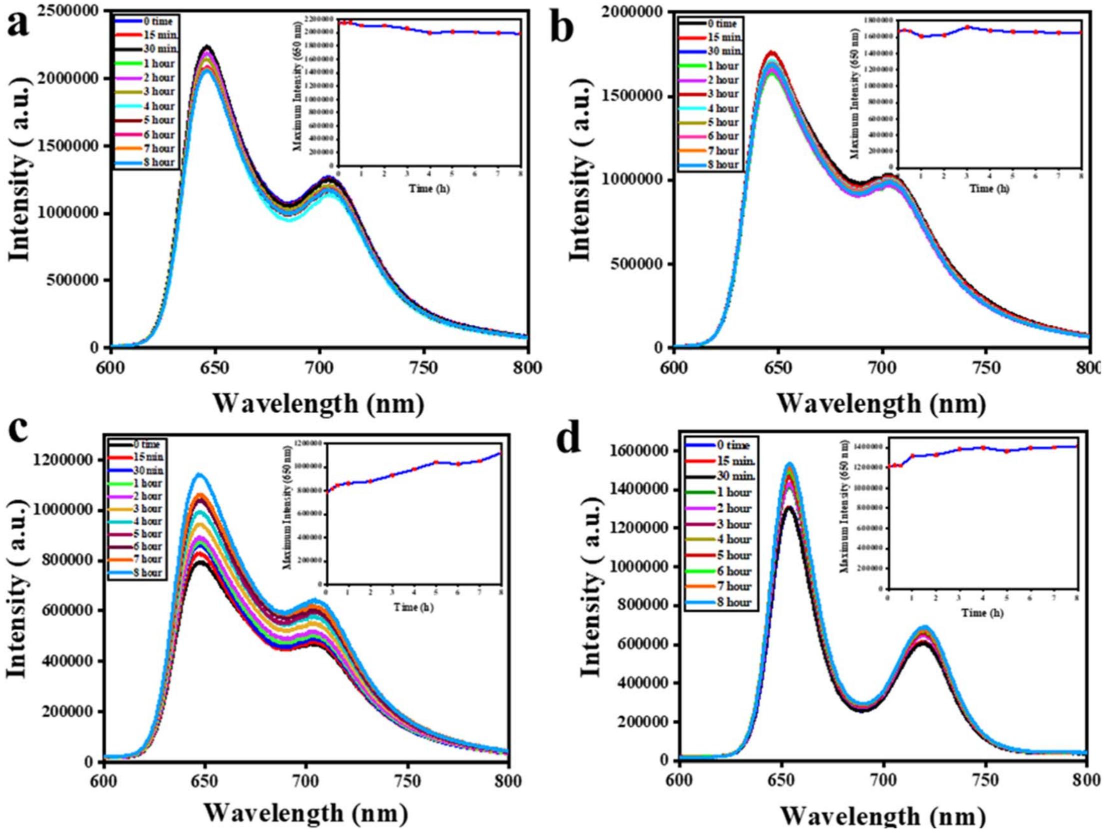

Fig. 4 Fluorescence stability evaluation of the porphyrin-derived CDs with incubation under different conditions including (a) deionized water (control), (b) PBS (pH = 7.4), (c) plain cell culture medium (DMEM), and (d) complete cell culture medium (10% serum) at different times intervals. (Insets) Plotting the maximum emission intensity ($\lambda_{em} = 650$ nm and $\lambda_{ex} = 419$ nm) against the corresponding measurement time.

enhance dispersion in various media and subsequently imply considerable stability of CDs.[37,38] Furthermore, many other factors including the tiny size and quasi-spherical structure of CDs, as well as the photostability of CDs may contribute to the noticeable fluorescence stability of the resultant CDs.[39,40]

The good photostability of CDs is considered one of the essential prerequisites for long-term biomedical applications including drug delivery and bioimaging purposes.[38,41,42] Herein, the photostability of the CDs was evaluated spectroscopically. As depicted in Fig. S5,† their UV-vis absorption spectra remained nearly unchanged after 24 minutes of continuous light exposure at 420 nm, demonstrating superior photostability compared to the parent porphyrin.[17,42] Consistent with earlier studies, our results confirm the excellent photostability of CDs obtained from various sources.[42–44]

3.3. Determination of fabricated CDs' water solubility and stability as well as lipophilicity

As demonstrated in Fig. S6,† the as-prepared CDs were found to be completely soluble in water up to a concentration of 2 mg mL^{-1} without any aggregation, unlike the starting porphyrin molecule which showed noticeable aggregation even at a very low concentration of 0.1 mg mL^{-1}. The DLS results also confirmed these findings (Fig. S7†), where the CDs exhibited non-significant aggregation with an average particle size of 32.67 nm at a concentration of 1 mg mL^{-1}. Moreover, the CDs showed favorable stability in the water, which was clarified by their UV-vis absorption spectra measurement over four consecutive days (Fig. 5a), where there was a non-significant change in their absorbance values (inset image). On the other hand, the lipophilicity assessment experiment revealed that the newly synthesized CDs are more lipophilic than the starting porphyrin molecule with average $\log P$ values of +0.66 ± 0.15 and +0.3 ± 0.09, respectively. These current findings indicated that porphyrin-derived CDs possess both hydrophilic and lipophilic properties as shown in Fig. S8,† which is consistent with the previously reported studies that verified the amphiphilic feature of the CDs.[45,46] Accordingly, they could improve the pharmacokinetic behaviors of DOX.[23]

3.4. Evaluation of DOX loading into and release from the porphyrin-based CDs

In our study, the effectiveness of the loading capacity as well as the release capability of the newly fabricated CDs as a promising nanocarrier tool for DOX was examined spectrophotometrically at 481 nm as previously described.[6] Herein, the DLE was found to be 93%, while DLC was measured to be 46.5 mg g^{-1}. These findings revealed that the as-prepared porphyrin-derived CDs possessed higher loading capacity and efficiency of DOX as compared to the previously reported findings.[6,12,23,24] The DOX

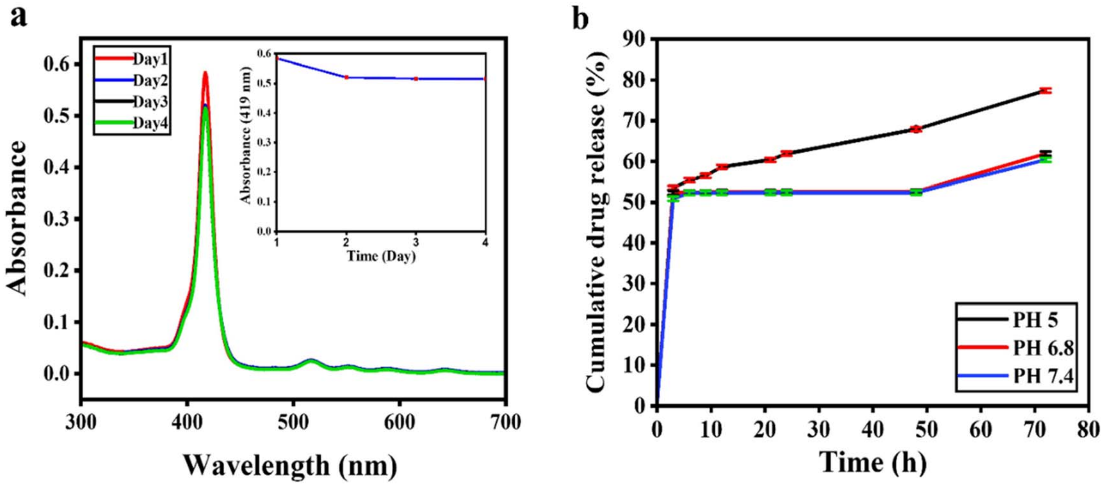

Fig. 5 (a) Spectroscopical evaluation of the synthesized CDs' water stability. (Inset) Plotting of the maximum absorbance value (at $\lambda = 419$ nm) against the corresponding time. (b) *In vitro* pH-dependent DOX release from the DOX@CDs nanocomposite at pH 5.0, 6.8, and 7.4, data are expressed as SD of mean and $n = 3$.

loading mechanism could be attributed to the electrostatic interaction between the multiple surface oxygen-rich functional groups of the synthesized CDs such as hydroxyl and carboxyl groups, and the amino group of DOX. In addition, the surface negative charge of the synthesized CDs as indicated by their zeta potential value, while the surface positive charge of DOX after dissolving in PBS (pH = 7.4) could also confirm the possibility of electrostatic attraction between the CDs and DOX. The CDs' outstanding hydrophilicity could also manipulate the hydrogen bond formation with DOX. Furthermore, the anthracene or phenyl rings of DOX could participate in π–π stacking interaction with the porphyrin-based CDs.[23,24,47]

On the other hand, the pH-dependent progressive DOX release from the designed DOX@CDs complex was examined at 3 different pH values 5.0, 6.8, and 7.4 which represented three distinct human tissue environments: the endothelium of cancer cells, the interstitial fluid of cancer cells, and the normal physiological environment, respectively. As shown in Fig. 5b, DOX was released at a significantly higher quantity at pH 5 compared to both pH 6.8 and 7.4. This could be attributed to the enhanced water solubility of DOX under acidic conditions expediting its release from the DOX@CDs composite as previously reported.[24] More importantly, after 72 hours, the cumulative percentage of DOX release was up to 77.4% at pH 5, whereas at pH 6.8 and 7.4, it reached 61.8 and 60.3%, respectively, which is consistent with the previously published data.[6,12,23,24] These findings verified that the DOX@CDs composite had a preferable DOX release capacity in acidic environments by which cancer cells are characterized, while a minimal release in physiological pH 7.4 and approximately neutral pH 6.8 characteristics for systemic circulation and normal cells, respectively, which is considered an excellent privilege for any DDS loaded with anticancer drugs to promote their therapeutic efficiency and simultaneously minimize their side effects.[24] Moreover, the DOX release was notably occurring at a relatively slow rate, where its release sustained until 72 h. Collectively, these findings revealed that the as-prepared DOX@CDs composite could be considered a promising DDS for selective DOX release within the tumor microenvironment to improve the anticancer therapeutic efficiency of DOX, in addition to the extended drug release which accordingly reduced the need for multiple dosing frequency with subsequent minimizing the serious adverse effects associated with frequent administration.[6,23,48]

3.5. Kinetics of *in vitro* DOX release

For a deeper understanding of the DOX release mechanism, three mathematical drug release models (zero order, first order, and Korsmeyer & Peppas models) were applied in the current study, utilizing data from the *in vitro* release experiment. The calculated various parameters from all studied models indicated that the DOX release from the DOX@CDs composite was best fitted to the Korsmeyer & Peppas (Fig. 6 and Table 1), which could be attributed to the polymeric-like structure of CDs as previously described.[49,50] Moreover, the exponent diffusion parameter (n) calculated from the Korsmeyer and Peppas equation was 0.108 at pH 5, which is less than 0.45, revealing that DOX release from porphyrin-derived CDs was controlled by the Fickian diffusion mechanism as previously indicated as well.[18,48,51]

3.6. Biocompatibility and cytotoxicity assessment

Despite DOX being a potent chemotherapeutic agent, its medical application as anticancer therapy is still suffering from many limitations, among them is the development of drug resistance, and induction of many serious adverse effects due to a narrow therapeutic index as well as lack of selectivity, where it cannot differentiate between normal and cancerous cells.[52–54] Therefore, it is favorable to utilize DDS that is non-toxic, biocompatible, and easily accessible to tumor cells to simultaneously minimize the associated adverse effects and improve the therapeutic efficacy of the loaded agent.[18] Among the variable DDS, CDs have been extensively utilized because of their

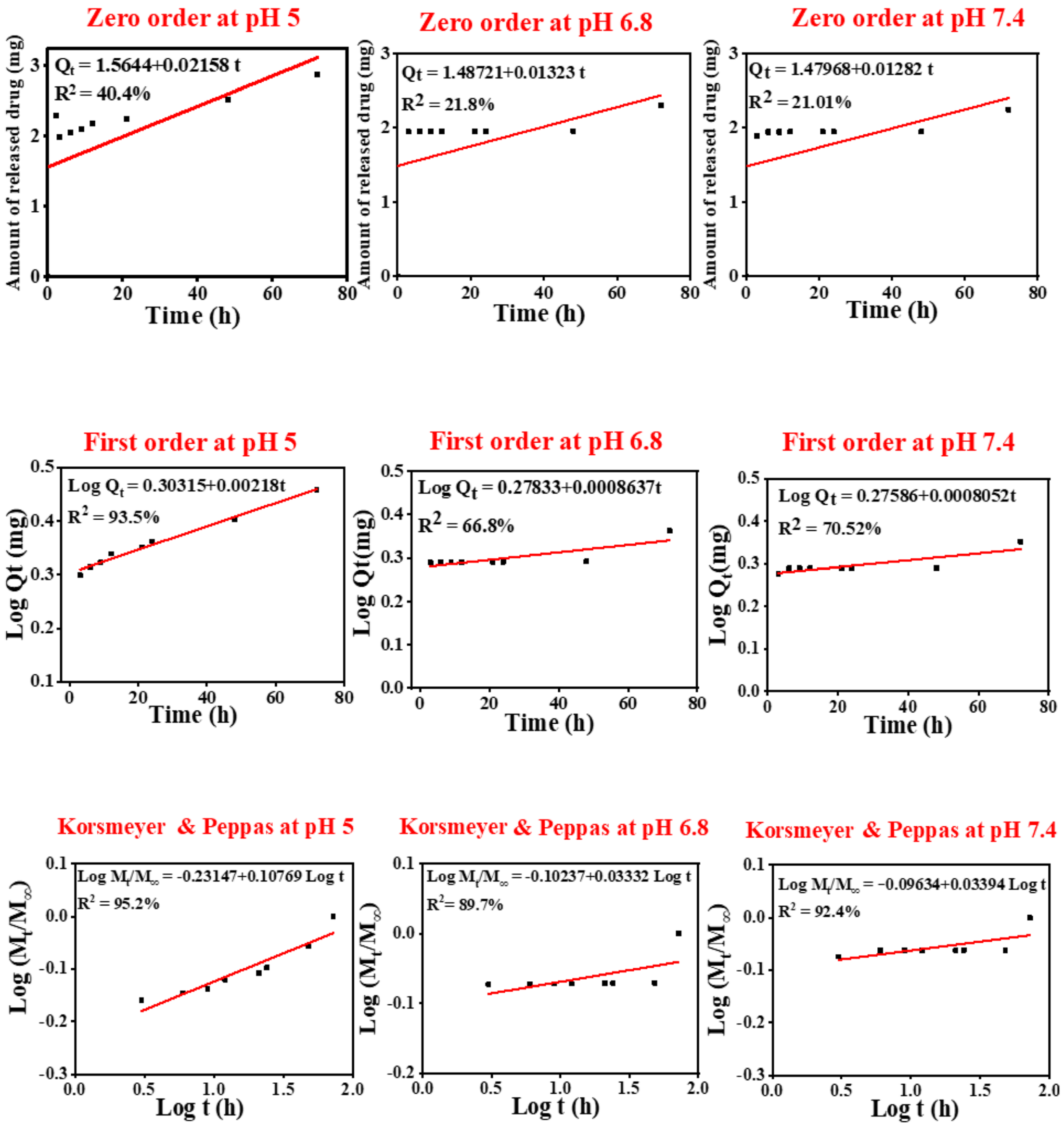

Fig. 6 Kinetics study of DOX release at pH 5.0, 6.8, and 7.4 by applying zero order, first order, and Korsmeyer and Peppas models.

excellent biocompatibility and safety.[12] As shown in Fig. 7a, the safety profile of the synthesized CDs, as well as the DOX@CDs complex were verified compared to the free DOX utilizing the MTT assay against RPE-1 cells, where the viability of RPE-1 cells was kept above 90% even at the highest utilized concentration (100 μg mL^{-1}) of both CDs and DOX@CDs, unlike the treatment by free Dox which showed a significant cytotoxic effect (cell viability = 60%) even at the lowest utilized concentration (6.25 μg mL^{-1}). These findings revealed that the as-prepared CDs are biocompatible and could be non-toxic DDS. Moreover, they could protect normal cells from DOX's cytotoxic effect with subsequent diminution of the associated side effects. Collectively, these results are compatible with the previously reported findings indicating that negligible cytotoxic behavior of DOX-

Table 1 Kinetic parameters calculation for mathematical models of DOX release at pH values of 5.0, 6.8, and 7.4

	pH = 5.0			pH = 6.8			pH = 7.4		
Model	R^2	K	n	R^2	K	n	R^2	K	n
Zero-order	40.4%	0.022	—	21.8%	0.013	—	21.01%	0.013	—
First-order	93.5%	0.005	—	66.8%	0.002	—	70.52%	0.002	—
Korsmeyer–Peppas	95.2%	0.586	0.108	89.7%	0.79	0.0333	92.4%	0.801	0.0339

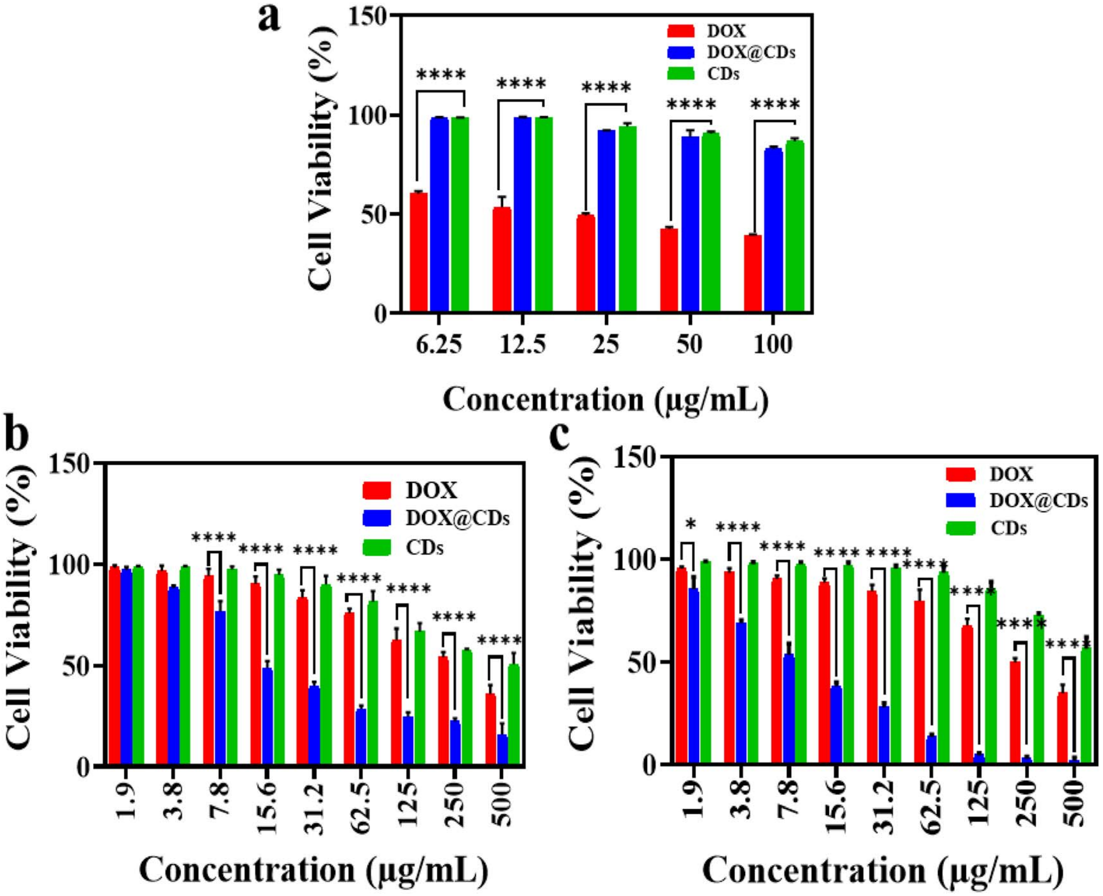

Fig. 7 MTT assay results. Biocompatibility testing of free DOX, CDs, and DOX@CDs complex against normal RPE-1 cells at concentrations 6.25, 12.5, 25, 50, and 100 µg mL^{-1} (a). The therapeutic anticancer effect of free DOX, CDs, and DOX@CDs against MCF-7 (b) and MDA-MB-231 (c) cells at concentrations 1.9, 3.8, 7.8, 15.6, 31.2, 62.5, 125, 250, and 500 µg mL^{-1}. The data are represented as M ± SD, $n = 3$, and ****$p < 0.0001$.

loaded CDs towards normal cells compared with the cancerous cells that could be ascribed to the selective pH-dependent DOX release.[24] Based on these findings, along with pharmacokinetic behaviors of the DOX@CDs complex in comparison with free DOX, the therapeutic efficacy was further investigated against human breast cancer cell lines MCF-7 and MDA-MB-231 as illustrated in Fig. 7b and c, respectively. Notably, the findings revealed that the DOX@CDs complex had a significantly more potent therapeutic effect against both MCF-7 and MDA-MB-231 cell lines compared to the free DOX. Furthermore, the cytotoxic effect of the DOX@CDs complex was found to be dose dependent.

The half maximal inhibitory concentration (IC_{50}) fitted curves for MCF-7 (Fig. 8a) demonstrated that the DOX@CDs complex induced 50% of cell death at a very low concentration compared to the free DOX, where the calculated IC_{50} values for DOX@CDs complex and free DOX were 24.08 ± 1.446 and 262.96 ± 1.807 µg mL^{-1}, respectively (~11 times higher therapeutic efficacy) as illustrated in Fig. 8b. Analogously, for MDA-MB-231, the DOX@CDs complex induced 50% of cell death at a significantly very low concentration compared to the free DOX (Fig. 8c), with IC_{50} values of 10.587 ± 0.815 and 261.6 ± 0.907 µg mL^{-1}, respectively (~24 times higher potency) as clarified in Fig. 8d. Moreover, the DOX@CDs complex exhibited 2.3 times higher cytotoxic action against the triple-negative human breast cancer cells (MDA-MB-231) than the MCF-7 cells, unlike the DOX which showed equal potency against both cells. These findings together verified the validity of the synthesized CDs to be a promising DDS for DOX which could be attributed to the enhanced cellular uptake of the tiny-sized CDs with subsequent effective transport, release into the cancer cells, and eventually synergistic therapeutic outcomes.[55]

3.7. Intracellular localization and uptake (fluorescence microscopy and flow cytometry analysis)

Herein, the cellular localization and internalization of MCF-7 and MDA-MB-231 cells for CDs, free DOX, and DOX@CDs complex was investigated by fluorescence microscopy and flow cytometry. As demonstrated in Fig. 9, the fluorescence images captured under green and red light for both MCF-7, and MDA-MB-231 cells incubated with CDs, free DOX, and DOX@CDs for 4 hours exhibited that CDs were mainly distributed in the cytoplasm and in the perinuclear region which resembled the localization behavior of free DOX. More importantly, the fluorescence intensity of cells treated with DOX@CDs complex under both green and red light was stronger than that in those

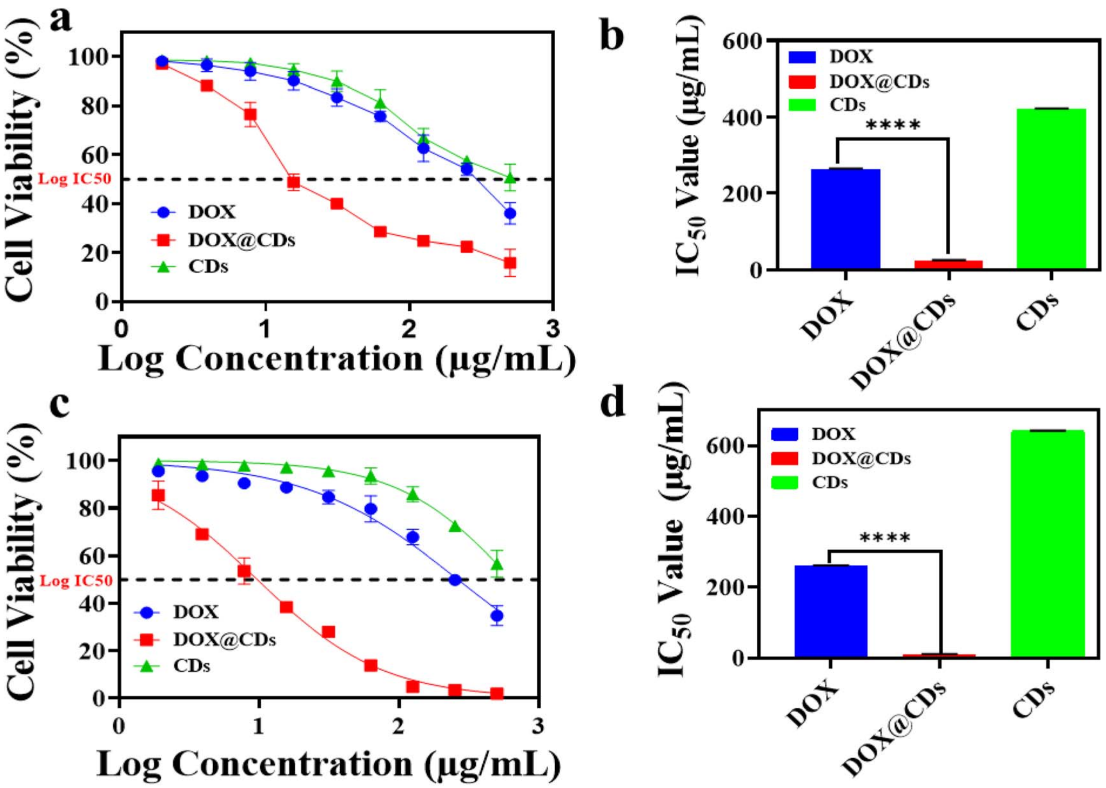

Fig. 8 Half maximal inhibition curves (a) and corresponding IC_{50} values (b) in µg mL^{-1} of free DOX, CDs, and DOX@CDs nanocomposite against MCF-7. Half maximal inhibition curves (c) and corresponding IC_{50} values (d) in µg mL^{-1} of free DOX, CDs, and DOX@CDs nanocomposite against MDA-MB-231 cells. The data are represented as M ± SD, $n = 3$, and $^{****}p < 0.0001$.

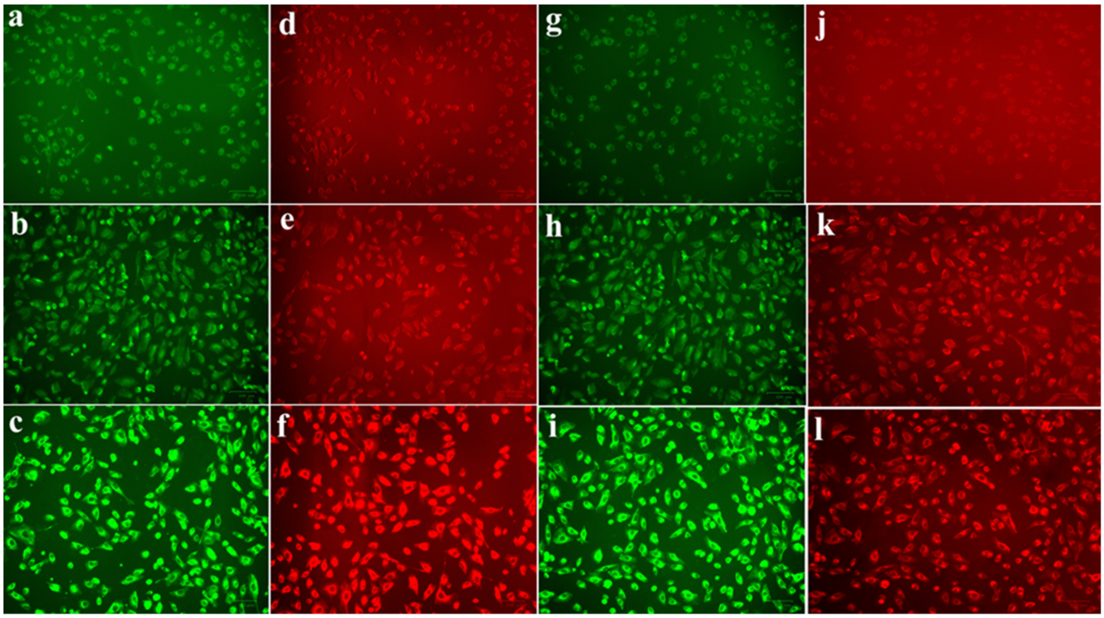

Fig. 9 Fluorescence microscopy imaging of MCF-7 cells (left) treated with CDs (a and d), free DOX (b and e), and DOX@CDs (c and f) and MDA-MB-231(right) treated with CDs (g and j), free DOX (h and k), and DOX@CDs (i and l) under green and red light, respectively. The cells were incubated for 4 hours at concentrations 250 µg mL^{-1} (CDs) and 260 µg mL^{-1} of DOX (for free DOX and DOX@CDs). The scale bar was 100 µm.

treated with free DOX indicating a higher cellular permeability and localization of the DOX@CDs. These findings comply with the above-described MTT assay results showing that DOX@CDs complex was more cytotoxic against breast cancer cells compared to the free DOX. Moreover, they are in good agreement with the previously reported studies verified that loading

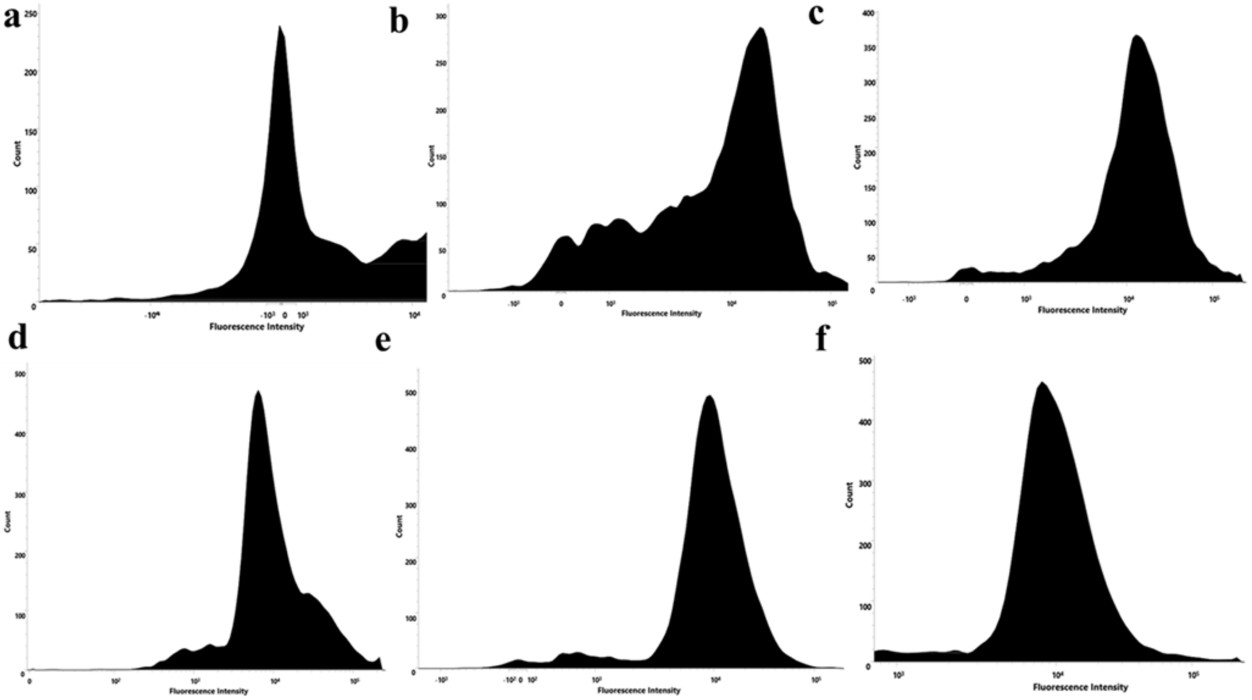

Fig. 10 Intracellular uptake by flow cytometry after 4 hours of incubation. MCF-7 and MDA-MB-231 cells treated with CDs (a and d), free DOX (b and e), and DOX@CDs (c and f) and at concentrations of 250 μg mL^{-1} and 260 μg mL^{-1} of DOX, respectively.

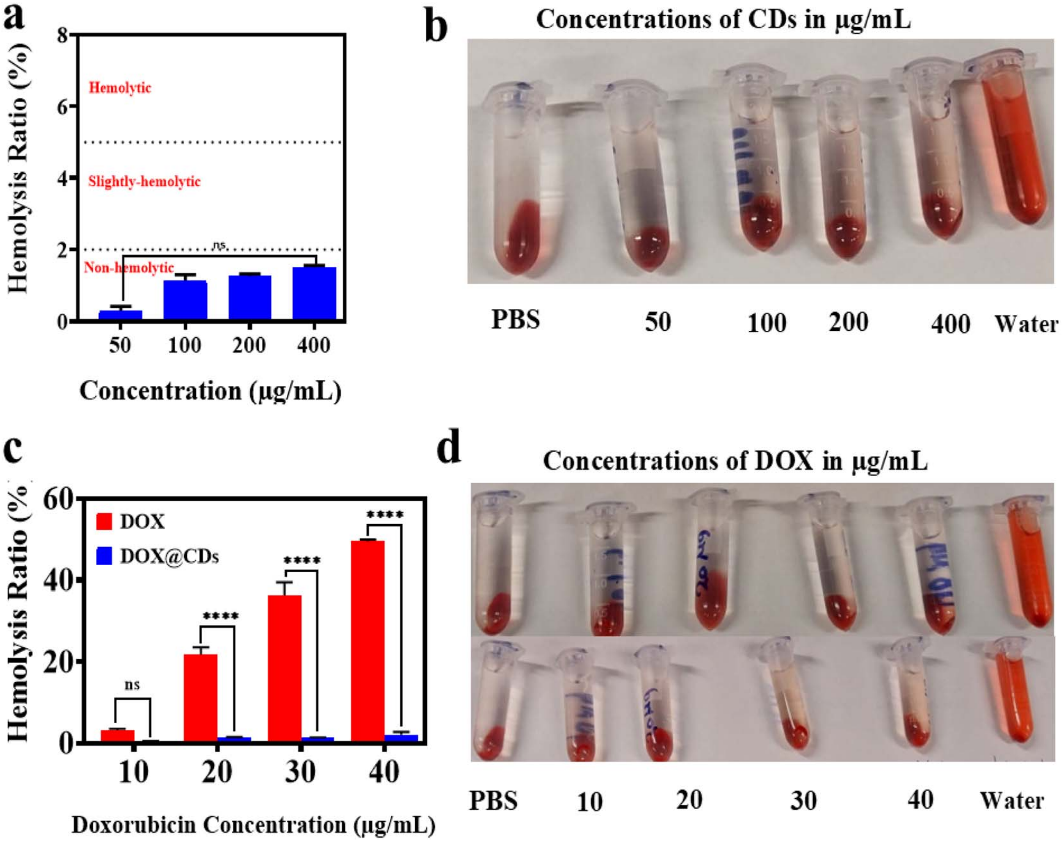

Fig. 11 (a) Hemolysis ratio of CDs at concentrations 50, 100, 200, and 400 μg mL^{-1}. (b) Photographs captured during the hemocompatibility assessment of CDs. (c) Hemolysis ratio of the free DOX in comparison with the DOX@CDs complex at concentrations 10, 20, 30, and 40 μg mL^{-1} of DOX. (d) Photographs captured during the hemolytic activity testing of the DOX@CDs complex (top) and free DOX (bottom). Deionized water and PBS were utilized as positive and negative controls, respectively, for all studied groups. The data are expressed as M ± SD, $n = 3$, ns (non-significant), and ****$p < 0.0001$.

DOX into CDs could be an efficient DDS maximizing the therapeutic efficacy of DOX against cancerous cells.[6,23,24]

The enhancement in the cellular internalization of breast cancer cells (MCF-7 and MDA-MB-231) to DOX@CDs complex compared to the free DOX was further verified by the flow cytometry analysis revealing that there was a higher uptake observed for DOX@CDs complex in comparison with the free DOX at the same DOX concentration and after the same incubation period as shown in Fig. 10. This was detected by the higher fluorescence intensity correlated with a higher cellular uptake in the DOX@CDs treated cells unlike those treated with free DOX. Notably, there was no significant variation in the cellular uptake between the two different incubation times as shown in Fig. S9.† Collectively, this augmentation in the cellular uptake for DOX@CDs compared to the free DOX as verified by qualitative and quantitative analysis could be attributed to the combination of two transportation mechanisms endocytosis and passive diffusion responsible for uptake of CDs into the cells unlike the free DOX which is transported into the cells through a single passive diffusion mechanism.[6,23,56]

3.8. Hemocompatibility assessment

Given the direct contact of therapeutic agents or biomaterials with the bloodstream, it's crucial to assess their *in vitro* blood compatibility prior to *in vivo* use. The hemolysis assay is a standard test for assessing a biomaterial's initial hemocompatibility.[57,58] Fig. 11a and b depict the hemolytic ratio and visual representation of various CD concentrations, respectively. Notably, no significant hemolysis of RBCs was observed across all CD concentrations tested compared to the negative control (PBS). The hemolytic ratio remained below the 2% safety threshold (ASTM F 756-00) even at the highest concentration, indicating excellent hemocompatibility.[57] In contrast, free DOX-induced dose-dependent RBC rupture, with hemolysis ratios reaching 21.8 ± 1.805%, 36.4 ± 3.088%, and 49.5 ± 0.456% at 20, 30, and 40 μg mL^{-1}, respectively (Fig. 11c and d, bottom).

Conversely, loading DOX into CDs significantly reduced hemolysis (Fig. 11c and d, top). Even at the highest DOX concentration (40 μg mL^{-1}), DOX@CDs maintained a hemolysis ratio below the safety threshold (1.32 ± 0.208%, 1.34 ± 0.092%, and 2.09 ± 0.705% at 20, 30, and 40 μg mL^{-1}, respectively), representing a 16-, 27-, and 23-fold decrease compared to free DOX. These findings align with previous reports highlighting the biocompatibility of CDs in blood systems and the protective effect of various DDS against DOX-induced hemolysis.[25,26,58–61]

4 Conclusions

We report a facile one-step solvothermal synthesis of novel porphyrin-derived carbon dots (CDs) using TCPP and urea as precursors. Subsequent non-covalent conjugation of doxorubicin (DOX) yielded pH-responsive DOX@CDs nanocomposites. The resulting CDs exhibited excellent water solubility, stability, and improved photostability compared to TCPP. The DOX@CDs complex demonstrated satisfactory drug loading and pH-dependent release, with accelerated release in acidic conditions, mimicking the tumor microenvironment. Notably, both CDs and DOX@CDs exhibited enhanced biocompatibility compared to free DOX, while maintaining potent cytotoxicity against breast cancer cells (MCF-7 and MDA-MB-231). Moreover, the loading of DOX into the porphyrin-derived CDs resulted in an efficient delivery with higher cellular uptake into the breast cancer cells. Additionally, the DOX@CDs complex mitigated the hemolytic effects of free DOX. In summary, this study establishes porphyrin-derived carbon dots (CDs) as a biocompatible nanocarrier system for the efficient delivery of doxorubicin (DOX) to human breast cancer cells. The resulting DOX-loaded CDs exhibited enhanced cytotoxicity and reduced systemic toxicity compared to free DOX.

Data availability

The datasets examined and collected will be made available upon request and all supporting data for this study are also available in the ESI.†

Conflicts of interest

The authors declare no conflicts of interest.

Acknowledgements

This work supported from the Science, Technology & Innovation Funding Authority (STDF) under grant number 46207. Abeer Ansary gratefully acknowledges the financial support provided by the Egyptian Ministry of Higher Education (MoHE) scholarship at Egypt-Japan University of Science and Technology (E-JUST) which also supported the research by providing the facilities and labs required to conduct this study.

References

1 A. Burguin, C. Diorio and F. Durocher, Breast Cancer Treatments: Updates and New Challenges, *J. Pers. Med.*, 2021, **11**, 808.
2 F. Bray, M. Laversanne, H. Sung, J. Ferlay, R. L. Siegel, I. Soerjomataram and A. Jemal, Global cancer statistics 2022: GLOBOCAN estimates of incidence and mortality worldwide for 36 cancers in 185 countries, *Ca-Cancer J. Clin.*, 2024, **74**, 229–263.
3 C. Christowitz, T. Davis, A. Isaacs, G. van Niekerk, S. Hattingh and A. M. Engelbrecht, Mechanisms of doxorubicin-induced drug resistance and drug resistant tumour growth in a murine breast tumour model, *BMC Cancer*, 2019, **19**, 757.
4 C. Carvalho, R. X. Santos, S. Cardoso, S. Correia, P. J. Oliveira, M. S. Santos and P. I. Moreira, Doxorubicin: the good, the bad and the ugly effect, *Curr. Med. Chem.*, 2009, **16**, 3267–3285.
5 L. Yang, Z. Wang, J. Wang, W. Jiang, X. Jiang, Z. Bai, Y. He, J. Jiang, D. Wang and L. Yang, Doxorubicin conjugated functionalizable carbon dots for nucleus targeted delivery

and enhanced therapeutic efficacy, *Nanoscale*, 2016, **8**, 6801–6809.

6 T. Kong, L. Hao, Y. Wei, X. Cai and B. Zhu, Doxorubicin conjugated carbon dots as a drug delivery system for human breast cancer therapy, *Cell Proliferation*, 2018, **51**, e12488.

7 Y. Wang, X. Wei, C. Zhang, F. Zhang and W. Liang, Nanoparticle delivery strategies to target doxorubicin to tumor cells and reduce side effects, *Ther. Delivery*, 2010, **1**, 273–287.

8 A. Shafei, W. El-Bakly, A. Sobhy, O. Wagdy, A. Reda, O. Aboelenin, A. Marzouk, K. El Habak, R. Mostafa, M. A. Ali and M. Ellithy, A review on the efficacy and toxicity of different doxorubicin nanoparticles for targeted therapy in metastatic breast cancer, *Biomed. Pharmacother.*, 2017, **95**, 1209–1218.

9 J. Lao, J. Madani, T. Puértolas, M. Alvarez, A. Hernández, R. Pazo-Cid, A. Artal and A. Antón Torres, Liposomal Doxorubicin in the treatment of breast cancer patients: a review, *J. Drug Delivery*, 2013, **2013**, 456409.

10 J. Liu, R. Li and B. Yang, Carbon Dots: A New Type of Carbon-Based Nanomaterial with Wide Applications, *ACS Cent. Sci.*, 2020, **6**, 2179–2195.

11 M. Behi, L. Gholami, S. Naficy, S. Palomba and F. Dehghani, Carbon dots: a novel platform for biomedical applications, *Nanoscale Adv.*, 2022, **4**, 353–376.

12 S. N. Dada, G. K. Babanyinah, M. T. Tetteh, V. E. Palau, Z. F. Walls, K. Krishnan, Z. Croft, A. U. Khan, G. Liu and T. E. Wiese, Covalent and noncovalent loading of doxorubicin by folic acid-carbon dot nanoparticles for cancer theranostics, *ACS Omega*, 2022, **7**, 23322–23331.

13 J. Gan, Y. Wu, F. Yang, X. Wu, Y. Wang and J. Wang, UV-filtering cellulose nanocrystal/carbon quantum dot composite films for light conversion in glass windows, *ACS Appl. Nano Mater.*, 2021, **4**, 12552–12560.

14 Z. Han, Y. Ni, J. Ren, W. Zhang, Y. Wang, Z. Xie, S. Zhou and S. F. Yu, Highly efficient and ultra-narrow bandwidth orange emissive carbon dots for microcavity lasers, *Nanoscale*, 2019, **11**, 11577–11583.

15 T. Li, L. Xie, R. Long, C. Tong, Y. Guo, X. Tong, S. Shi and Q. Lin, Cetyltrimethyl ammonium mediated enhancement of the red emission of carbon dots and an advanced method for fluorometric determination of iron (III), *Mikrochim. Acta*, 2019, **186**, 1–8.

16 J. Zeng, L. Liao, X. Lin, G. Liu, X. Luo, M. Luo and F. Wu, Red-emissive sulfur-doped carbon dots for selective and sensitive detection of mercury (II) ion and glutathione, *Int. J. Mol. Sci.*, 2022, **23**, 9213.

17 Y. Li, X. Zheng, X. Zhang, S. Liu, Q. Pei, M. Zheng and Z. Xie, Porphyrin-based carbon dots for photodynamic therapy of hepatoma, *Adv. Healthcare Mater.*, 2017, **6**, 1600924.

18 E. Serag, M. Helal and A. El Nemr, Curcumin Loaded onto Folic acid Carbon dots as a Potent drug Delivery System for Antibacterial and Anticancer Applications, *J. Cluster Sci.*, 2024, **35**, 519–532.

19 P. G. Mahajan, N. C. Dige, B. D. Vanjare, A. Phull, S. J. Kim, S.-K. Hong and K. H. Lee, Synthesis, photophysical properties and application of new porphyrin derivatives for use in photodynamic therapy and cell imaging, *J. Fluoresc.*, 2018, **28**, 871–882.

20 H. Ishida, S. Tobita, Y. Hasegawa, R. Katoh and K. Nozaki, Recent advances in instrumentation for absolute emission quantum yield measurements, *Coord. Chem. Rev.*, 2010, **254**, 2449–2458.

21 K. Mousa, A. Abd El-Moneim, S. F El-Mashtoly, M. M. Mohamed and M. E. El-Khouly, Laser-induced graphene functionalized cationic porphyrin: fabrication, characterization, and intra-supramolecular electron transfer process, *RSC Adv.*, 2025, **15**, 289–300.

22 D. Kempińska, T. Chmiel, A. Kot-Wasik, A. Mroz, Z. Mazerska and J. Namieśnik, State of the art and prospects of methods for determination of lipophilicity of chemical compounds, TrAC, *Trends Anal. Chem.*, 2019, **113**, 54–73.

23 Y. Yuan, B. Guo, L. Hao, N. Liu, Y. Lin, W. Guo, X. Li and B. Gu, Doxorubicin-loaded environmentally friendly carbon dots as a novel drug delivery system for nucleus targeted cancer therapy, *Colloids Surf., B*, 2017, **159**, 349–359.

24 Y. Hailing, L. Xiufang, W. Lili, L. Baoqiang, H. Kaichen, H. Yongquan, Z. Qianqian, M. Chaoming, R. Xiaoshuai and Z. Rui, Doxorubicin-loaded fluorescent carbon dots with PEI passivation as a drug delivery system for cancer therapy, *Nanoscale*, 2020, **12**, 17222–17237.

25 H. Cheng, Y. Zhao, Y. Wang, Y. Hou, R. Zhang, M. Zong, L. Sun, Y. Liu, J. Qi, X. Wu and B. Li, The Potential of Novel Synthesized Carbon Dots Derived Resveratrol Using One-Pot Green Method in Accelerating in vivo Wound Healing, *Int. J. Nanomed.*, 2023, **18**, 6813–6828.

26 M. A. Khan, A. N. Aljarbou, Y. H. Aldebasi, M. S. Alorainy and A. Khan, Combination of glycosphingosomes and liposomal doxorubicin shows increased activity against dimethyl-α-benzanthracene-induced fibrosarcoma in mice, *Int. J. Nanomed.*, 2015, **10**, 6331–6338.

27 L. Mazzarino, G. Loch-Neckel, L. Dos Santos Bubniak, F. Ourique, I. Otsuka, S. Halila, R. Curi Pedrosa, M. C. Santos-Silva, E. Lemos-Senna, E. Curti Muniz and R. Borsali, Nanoparticles Made From Xyloglucan-Block-Polycaprolactone Copolymers: Safety Assessment for Drug Delivery, *Toxicol. Sci.*, 2015, **147**, 104–115.

28 X. Xie, D. Li, Y. Chen, Y. Shen, F. Yu, W. Wang, Z. Yuan, Y. Morsi, J. Wu and X. Mo, Conjugate Electrospun 3D Gelatin Nanofiber Sponge for Rapid Hemostasis, *Adv. Healthcare Mater.*, 2021, **10**, e2100918.

29 C. Huang, H. Dong, Y. Su, Y. Wu, R. Narron and Q. Yong, Synthesis of carbon quantum dot nanoparticles derived from byproducts in bio-refinery process for cell imaging and in vivo bioimaging, *Nanomaterials*, 2019, **9**, 387.

30 V. Selvamani, Stability studies on nanomaterials used in drugs, *Characterization and Biology of Nanomaterials for Drug Delivery*, Elsevier, 2019, pp. 425–444.

31 E. Faghfuri, M. Sagha and A. H. Faghfouri, The cytotoxicity effect of curcumin loaded folic acid conjugated-nanoparticles on breast cancer cells and its association

with inhibition of STAT3 phosphorylation, *J. Cluster Sci.*, 2022, **33**, 2037–2044.

32 T. N. Nguyen, T. T. Nguyen, T. H. L. Nghiem, D. T. Nguyen, T. H. Tran, D. Vu, T. B. N. Nguyen, T. M. H. Nguyen, V. T. Nguyen and M. H. Nguyen, Optical properties of doxorubicin hydrochloride load and release on silica nanoparticle platform, *Molecules*, 2021, **26**, 3968.

33 J. Wu, W. Wang and Z. Wang, Porphin-based carbon dots for "turn off–on" phosphate sensing and cell imaging, *Nanomaterials*, 2020, **10**, 326.

34 Q. Q. Zhang, B. B. Chen, H. Y. Zou, Y. F. Li and C. Z. Huang, Inner filter with carbon quantum dots: A selective sensing platform for detection of hematin in human red cells, *Biosens. Bioelectron.*, 2018, **100**, 148–154.

35 N. Gao, W. Yang, H. Nie, Y. Gong, J. Jing, L. Gao and X. Zhang, Turn-on theranostic fluorescent nanoprobe by electrostatic self-assembly of carbon dots with doxorubicin for targeted cancer cell imaging, in vivo hyaluronidase analysis, and targeted drug delivery, *Biosens. Bioelectron.*, 2017, **96**, 300–307.

36 J. Ge, Q. Jia, W. Liu, L. Guo, Q. Liu, M. Lan, H. Zhang, X. Meng and P. Wang, Red-Emissive Carbon Dots for Fluorescent, Photoacoustic, and Thermal Theranostics in Living Mice, *Adv. Mater.*, 2015, **27**, 4169–4177.

37 F. Yan, Z. Sun, H. Zhang, X. Sun, Y. Jiang and Z. Bai, The fluorescence mechanism of carbon dots, and methods for tuning their emission color: a review, *Mikrochim. Acta*, 2019, **186**, 1–37.

38 S. Dua, P. Kumar, B. Pani, A. Kaur, M. Khanna and G. Bhatt, Stability of carbon quantum dots: a critical review, *RSC Adv.*, 2023, **13**, 13845–13861.

39 A. M. El-Shafey, Carbon dots: Discovery, structure, fluorescent properties, and applications, *Green Process. Synth.*, 2021, **10**, 134–156.

40 Y. An, Z. Wang and F.-G. Wu, Fluorescent carbon dots for discriminating cell types: a review, *Anal. Bioanal. Chem.*, 2024, **416**, 3945–3962.

41 L. Cui, X. Ren, M. Sun, H. Liu and L. Xia, Carbon Dots: Synthesis, Properties and Applications, *Nanomaterials*, 2021, **11**, 3419.

42 D. Ozyurt, M. Al Kobaisi, R. K. Hocking and B. Fox, Properties, synthesis, and applications of carbon dots: A review, *Carbon Trends*, 2023, **12**, 100276.

43 Z. Zhao, B. Pieber and M. Delbianco, Modulating the surface and photophysical properties of carbon dots to access colloidal photocatalysts for cross-couplings, *ACS Catal.*, 2022, **12**, 13831–13837.

44 K.-W. Chu, S. L. Lee, C. i.-J. Chang and L. Liu, Recent progress of carbon dot precursors and photocatalysis applications, *Polymers*, 2019, **11**, 689.

45 M. Ortega-Munoz, P. Vargas-Navarro, S. Plesselova, M. D. Giron-Gonzalez, G. R. Iglesias, R. Salto-Gonzalez, F. Hernandez-Mateo, A. V. Delgado, F. J. Lopez-Jaramillo and F. Santoyo-Gonzalez, Amphiphilic-like carbon dots as antitumoral drug vehicles and phototherapeutical agents, *Mater. Chem. Front.*, 2021, **5**, 8151–8160.

46 S. A. Cherevkov, E. A. Stepanidenko, M. D. Miruschenko, A. M. Zverkov, A. M. Mitroshin, I. V. Margaryan, I. G. Spiridonov, D. V. Danilov, A. V. Koroleva and E. V. Zhizhin, Amphiphilic acetylacetone-based carbon dots, *J. Mater. Chem. C*, 2024, **12**, 3943–3952.

47 T. T. A. Do, K. Wicaksono, A. Soendoro, T. Imae, M. J. Garcia-Celma and S. Grijalvo, Complexation Nanoarchitectonics of Carbon Dots with Doxorubicin toward Photodynamic Anti-Cancer Therapy, *J. Funct. Biomater.*, 2022, **13**, 219.

48 S. Zhou, X. Zheng, K. Yi, X. Du, C. Wang, P. Cui, P. Jiang, X. Ni, L. Qiu and J. Wang, Temperature-Ion-pH Triple Responsive Gellan Gum as In Situ Hydrogel for Long-Acting Cancer Treatment, *Gels*, 2022, **8**, 508.

49 M. Z. Fahmi, Y. Y. Aung, M. A. Ahmad, A. N. Kristanti, S. C. W. Sakti, O. P. Arjasa and H. V. Lee, In vivo Study of Chalcone Loaded Carbon Dots for Enhancement of Anticancer and Bioimaging Potencies, *Nanotheranostics*, 2023, **7**, 281–298.

50 F. Shafiei, M. Ghavami-Lahiji, T. S. Jafarzadeh Kashi and F. Najafi, Drug release kinetics and biological properties of a novel local drug carrier system, *Dent. Res. J.*, 2021, **18**, 94.

51 D. Chudoba, M. Jażdżewska, K. Łudzik, S. Wołoszczuk, E. Juszyńska-Gałązka and M. Kościński, Description of Release Process of Doxorubicin from Modified Carbon Nanotubes, *Int. J. Mol. Sci.*, 2021, **22**, 12003.

52 S. Peter, S. Alven, R. B. Maseko and B. A. Aderibigbe, Doxorubicin-Based Hybrid Compounds as Potential Anticancer Agents: A Review, *Molecules*, 2022, **27**, 4478.

53 N. Akhtar, H. A. Mohammed, M. Yusuf, A. Al-Subaiyel, G. M. Sulaiman and R. A. Khan, SPIONs Conjugate Supported Anticancer Drug Doxorubicin's Delivery: Current Status, Challenges, and Prospects, *Nanomaterials*, 2022, **12**, 3686.

54 A. Bisht, D. Avinash, K. K. Sahu, P. Patel, G. Das Gupta and B. D. Kurmi, A comprehensive review on doxorubicin: mechanisms, toxicity, clinical trials, combination therapies and nanoformulations in breast cancer, Drug delivery and translational research, *Drug Delivery Transl. Res.*, 2024, **15**, 102–133.

55 D. Wang, X. Li, X. Li, A. Kang, L. Sun, M. Sun, F. Yang and C. Xu, Magnetic And pH Dual-Responsive Nanoparticles For Synergistic Drug-Resistant Breast Cancer Chemo/Photodynamic Therapy, *Int. J. Nanomed.*, 2019, **14**, 7665–7679.

56 L. Yang, Z. Wang, J. Wang, W. Jiang, X. Jiang, Z. Bai, Y. He, J. Jiang, D. Wang and L. Yang, Doxorubicin conjugated functionalizable carbon dots for nucleus targeted delivery and enhanced therapeutic efficacy, *Nanoscale*, 2016, **8**, 6801–6819.

57 A. M. Abd El-Aziz, E. Serag and M. E. El-Khouly, NIR light-triggered photodynamic antibacterial nanofiber membrane based on polycaprolactone and phthalocyanine derivative for biomedical applications, *RSC Adv.*, 2024, **14**, 24424–24437.

58 F. Sajjad, Y. J. Yan, D. Margetić and Z. L. Chen, Synthesis and in vitro PDT evaluation of red emission polymer dots (R-

CPDs) and pyropheophorbide-α conjugates, *Sci. Rep.*, 2021, **11**, 10013.

59 B. Han, L. Shen, H. Xie, Q. Huang, D. Zhao, X. Huang, X. Chen and J. Li, Synthesis of Carbon Dots with Hemostatic Effects Using Traditional Chinese Medicine as a Biomass Carbon Source, *ACS Omega*, 2023, **8**, 3176–3183.

60 J. Li, M. Li, L. Tian, Y. Qiu, Q. Yu, X. Wang, R. Guo and Q. He, Facile strategy by hyaluronic acid functional carbon dot-doxorubicin nanoparticles for CD44 targeted drug delivery and enhanced breast cancer therapy, *Int. J. Pharm.*, 2020, **578**, 119122.

61 M. Zhang, P. Yuan, N. Zhou, Y. Su, M. Shao and C. Chi, pH-Sensitive N-doped carbon dots–heparin and doxorubicin drug delivery system: preparation and anticancer research, *RSC Adv.*, 2017, **7**, 9347–9356.